JGR Atmospheres

RESEARCH ARTICLE
10.1029/2021JD036340

When Do Subpollen Particles Become Relevant for Ice Nucleation Processes in Clouds?

Sven Werchner[1], E. Gute[2,3], C. Hoose[1], Ch. Kottmeier[1], A. Pauling[4], H. Vogel[1], and B. Vogel[1]

[1]Institute of Meteorology and Climate Research, Karlsruhe Institute of Technology, Karlsruhe, Germany, [2]Department of Chemistry, University of Toronto, Toronto, ON, Canada, [3]Now at Department of Space, Earth and Environment, Chalmers University of Technology, Gothenburg, Sweden, [4]Federal Office of Meteorology and Climatology MeteoSwiss, Zurich, Switzerland

Abstract When exposed to sufficiently humid environments, pollen grains burst and release large quantities of small subpollen particles (SPPs) which carry ice nucleating macromolecules. In this study, for the first time we develop a physically based parameterization describing the bursting process of pollen by applying a turgor pressure parameterization and quantify the impact SPPs have on overall ice nucleation in clouds. SPPs are generated from simulated birch pollen emissions over Europe for a 10-day case study in spring. We found SPP concentrations to surpass pollen grain concentrations by 4–6 orders of magnitude leading to an abundance of biological ice nuclei from SPPs in the range of 10^3–10^4 m^{-3}. However, it is found that these concentrations lead to only small changes in hydrometeor number densities and precipitation. Addressing the question when SPPs become relevant for ice nucleation in clouds, we conducted a sensitivity investigation. We find that amplifying ice nucleation efficiency of biological particles by factors greater 100 increases the ice particle numbers by up to 25% ($T \approx 268$ K). Strong reductions show in cloud droplet number concentration and water vapor at these temperatures while water vapor is increasing at 600 m. Overall, we found a net reduction of water in the atmosphere as liquid and particularly water vapor density is reduced, while frozen water mass density increases above 257 K. Findings indicate an alteration of mixed-phase cloud composition and increased precipitation (up to 6.2%) when SPPs are considered as highly efficient biological ice nuclei.

Key Points:

- Subpollen particles (SPPs) reach freezing altitudes in large number concentrations
- Nucleation efficiency of SPPs affects both amplitude and sign of impact on nucleation processes
- Relevant impact requires greatly increased nucleation efficiency of the SPPs

Correspondence to:
S. Werchner,
Sven.Werchner@kit.edu

Citation:
Werchner, S., Gute, E., Hoose, C., Kottmeier, C., Pauling, A., Vogel, H., & Vogel, B. (2022). When do subpollen particles become relevant for ice nucleation processes in clouds? *Journal of Geophysical Research: Atmospheres*, *127*, e2021JD036340. https://doi.org/10.1029/2021JD036340

Received 10 DEC 2021
Accepted 24 JUL 2022

Sven Werchner and Ellen Gute contributed equally to this work.

Author Contributions:
Conceptualization: Sven Werchner, E. Gute, C. Hoose, A. Pauling, H. Vogel, B. Vogel
Data curation: Sven Werchner
Formal analysis: Sven Werchner, E. Gute, B. Vogel
Funding acquisition: E. Gute, C. Hoose, Ch. Kottmeier, H. Vogel, B. Vogel
Investigation: Sven Werchner, E. Gute, B. Vogel
Methodology: Sven Werchner, A. Pauling, H. Vogel, B. Vogel
Project Administration: E. Gute, C. Hoose, Ch. Kottmeier, H. Vogel, B. Vogel
Resources: Ch. Kottmeier, A. Pauling, H. Vogel
Software: Sven Werchner

1. Introduction

Biological ice-nucleating particles (INPs) are among the most efficient ice nuclei enabling ice formation in the atmosphere at high sub-zero temperatures (Hoose & Möhler, 2012). However, ice forming processes initiated by biogenic INPs are rarely considered nor sufficiently described in weather and climate models (Huang et al., 2021); largely due to the complexity and thus challenges to describe their emission fluxes and physical properties (Després et al., 2012; Fröhlich-Nowoisky et al., 2016).

Pollen grains are biological particles emitted into the atmosphere from plants in large quantities with estimated emission rates from 44 (Hoose et al., 2010) up to 84.5 Tg yr^{-1} (Jacobson & Streets, 2009) globally. The overall global fraction of biological INPs (considering pollen, bacteria, and fungal spores) was quantified to about 10^{-5}% relative to all heterogeneous INPs using a global model (Hoose et al., 2010). Primarily the generally large size of pollen grains (e.g., birch pollen grains have diameters of approx. 22 µm (Schäppi et al., 1997)) is considered to further diminish the relevance of pollen as INPs particularly in remote atmospheric regions such as high altitudes and regions without major vegetation (Steiner et al., 2015). However, more recently subpollen particles (SPPs), defined as smaller entities released or separated from the larger pollen grains, receive greater attention regarding their atmospheric relevance, particularly as cloud condensation nuclei (CCN) (Steiner et al., 2015; Wozniak et al., 2018) and INPs (Gute & Abbatt, 2020; O'Sullivan et al., 2015; Pummer et al., 2012). In fact, the ice nucleation ability of pollen and particularly SPPs is identified by several studies to range over several degrees Celsius for their median freezing temperature T_{50} where 50% of sample aliquots are frozen in droplet freezing experiments (see Gute and Abbatt (2020) for an overview of experimental studies investigating the ice nucleation ability of different pollen types). A recent study by Burkart et al. (2021) investigated the origin of the SPPs' ice nucleation ability. The study defined starch granules as SPP, which were found unable to nucleate ice themselves, but act as carrier for ice nucleating molecules. In the present study, we assume that the SPPs are coated sufficiently with ice nucleating molecules to nucleate ice.

Supervision: E. Gute, C. Hoose, Ch. Kottmeier, H. Vogel, B. Vogel
Validation: Sven Werchner, E. Gute, B. Vogel
Visualization: Sven Werchner, E. Gute, B. Vogel
Writing – original draft: Sven Werchner
Writing – review & editing: Sven Werchner, E. Gute, C. Hoose, Ch. Kottmeier, A. Pauling, H. Vogel, B. Vogel

Pollen bursting and the release of SPPs is found to occur when the pollen grains are exposed to high relative humidity (RH) (Taylor et al., 2004) or rainwater (Grote et al., 2003), although the necessity of liquid water being present to initiate pollen bursting remains unclear. However, higher RH is found to lead to a faster and greater number of pollen grains to burst and the subsequent release of SPPs (Zhou, 2014). SPPs generally show sizes between a few nanometers and a few micrometers (Bacsi et al., 2006; Taylor et al., 2004), thus having a diameter more than one order of magnitude smaller than pollen grains and approximately 1,000 SPPs per pollen grain are produced (Steiner et al., 2015).

Despite these cloud relevant properties of pollen and their SPPs, research interest in pollen is mostly centered around the adverse health effects of pollen allergens on humans. This interest in the effects of pollen on human health has led to warning systems for atmospheric pollen loads being established. Specifically, numerical pollen forecast models have been developed and are already in operational use, for example, in Switzerland and Germany (Baklanov et al., 2017; Sofiev et al., 2015; Vogel et al., 2008; Wang et al., 2017; Zhang et al., 2013; Zink et al., 2013). To forecast atmospheric pollen loads, these models include detailed parameterizations of pollen emission and washout processes, while other atmospheric interactions involving pollen, particularly in clouds, are to date largely neglected in operational applications.

This study is motivated by both the interest in understanding pollen loads in the atmosphere to assess health effects on humans, for example, the phenomenon of "Thunderstorm Asthma" and the interest in understanding pollen contributions to cloud processes. Thunderstorm asthma refers to an increase of asthma cases during heavy precipitation events (Suphioglu, 1998) where it is suggested that the bursting of pollen grains and the subsequent release of SPPs generates large amounts of small airborne allergen loaded particles affecting the human respiratory system. Besides further penetration of the small SPPs into the human lung, their smaller size compared to full pollen grains enables them to be transported to higher altitudes. Here, they may have a significant impact on atmospheric ice formation processes given similar ice nucleating properties of the carried ice nucleating molecules compared to the pollen grain itself (Burkart et al., 2021; Hader et al., 2014; O'Sullivan et al., 2015). A study on the role of pollen bursting on the production of CCN suggests that CCN number concentrations could increase by 10^2–10^3 cm^{-3} if pollen grains release SPPs (Steiner et al., 2015). Looking at the effects of SPP release on cloud and specifically precipitation processes, a follow-up study found high SPP numbers to suppress average seasonal precipitation by 32% during the spring pollen season in the United States (Wozniak et al., 2018).

While these few studies focus on the impact of SPPs on CCN, we investigate the effects of SPPs on ice nucleation, using an operational weather forecast model to address three questions: (a) *How high are SPP concentrations throughout the troposphere*?, (b) *Do SPPs have a significant impact on the amount of ice formed in mixed-phase clouds*?, and (c) *How does this affect precipitation*? To address these questions, we developed a parameterization for SPP generation from pollen bursting which is explained in Section 2 introducing the physical background and technical realization. In this section we also describe the model and simulation configuration. Study results are presented in Section 3 and we close the paper with a summary in Section 4.

2. Model Description

In this study, we are using the ICON-ART model, which is an extension of the "ICOsahedral Non-hydrostatic (ICON) modeling framework" (Zängl et al., 2015) by the Aerosol and Reactive Trace gas (ART) module (Rieger et al., 2015). ICON is a model system, developed by the German Weather Service (DWD) and the Max Planck Institute of Meteorology with the intention to unify the treatment of global weather prediction and climate modeling (Giorgetta et al., 2018). ICON operates on an unstructured triangular grid, which is generated by the continuous refinement of a spherical icosahedron projected onto the Earth's surface. ICON-ART accounts for chemical processes in both troposphere and stratosphere, aerosol chemistry and dynamics, and considers the effect of trace gases and aerosols on radiation and clouds (Gasch et al., 2017; Hoshyaripour et al., 2019; Rieger et al., 2015, 2017; Schröter et al., 2018).

The birch pollen emission parameterization in ICON-ART is based on the EMPOL-parameterization originally developed within the COSMO-ART (Consortium for Small-scale Modelling) framework (Zink et al., 2013). The latter is in operational use at MeteoSwiss (Pauling et al., 2020) and at the DWD for alder, birch, grass, and ragweed pollen forecast. The emitted pollen in the model have a monodisperse size distribution with a diameter

of 20 μm and details about the treatment of sedimentation and washout of the pollen can be found elsewhere (Vogel et al., 2008).

2.1. Parameterization of SPP Emission From Pollen Bursting

Here, we present a new parameterization for pollen bursting and SPP generation based on physical assumptions. Pollen bursting is driven by the turgor pressure, a positive hydrostatic pressure inside the pollen grain acting on the pollen wall (Lüttge & Kluge, 2012). The turgor pressure increases when the water potential of the ambient air (predominantly determined by the RH) is greater than the water potential of the pollen cytoplasm, resulting in a water flux into the pollen grain via osmotic processes. Subsequently, the pollen grain swells while the swelling is limited by the pollen wall which allows for a maximum change in radius of 1–2 μm (Zhou, 2014). Further water flux into the pollen grain compresses its cytoplasm and thereby increases the turgor pressure. The water influx stalls when the water potential inside the pollen grain equals the ambient water potential and maximum turgor pressure is reached or the turgor pressure exceeds the wall strength and the pollen grain bursts (Zhou, 2014).

Parameterizing pollen bursting for its implementation in the ICON-ART model requires the derivation of the temporal development of the turgor pressure p_T and a way of translating the turgor pressure into a burst fraction. The turgor pressure increases by a water flux into the already fully swollen pollen grain where the flux J in $m^3\ s^{-1}$ was described previously by Zhou (2014) depending on A the surface area of the pollen grain in m^2 and k the water permeability in $m\ s^{-1}\ Pa^{-1}$

$$J = Ak(\Delta\pi - (p_T - p_a)). \tag{1}$$

The difference between the water potential outside and the osmotic potential inside the pollen grain is represented by $\Delta\pi = \pi_{out} - \pi_{in}$ in Pa as is the difference between turgor pressure and atmospheric pressure p_a. According to Zhou (2014), the change in turgor pressure caused by water flux at time t with the compression module $E = 2.15 \cdot 10^9\ N\ m^{-2}$, the densities of the pollen cytoplasm before ρ_t and after the water flux entering the pollen grain $\rho_{t+\Delta t}$ in $kg\ m^{-3}$, and the time step Δt is

$$\Delta p_{T,t} = E\left(1 - \frac{\rho_t}{\rho_{t+\Delta t}}\right). \tag{2}$$

Due to the inability of the pollen grain to expand further as they are already fully swollen, its volume stays constant and the density ratio can be replaced by the corresponding mass ratio. Assuming the change in mass being small in comparison to the total mass itself, Equation 2 simplifies to

$$\Delta p_{T,t} = E\left(1 - \frac{m_t}{m_{t+\Delta t}}\right) \approx E\frac{\Delta m_t}{m_t}, \tag{3}$$

where the term Δm_t represents the change in mass caused by the previously described water flux ($\Delta m_t = J\rho_w \Delta t$) and can be determined by applying Equation 1 yielding

$$\Delta p_{T,t} = \frac{E}{m_t} Ak(\Delta\pi - p_{T,t} + p_a)\rho_w \Delta t \tag{4}$$

with the water density ρ_w in $kg\ m^{-3}$. Equation 4 is transformed into the following differential equation for the temporal development of the turgor pressure:

$$\frac{dp_T}{dt} = \frac{E}{m} Ak(\Delta\pi - p_T + p_a)\rho_w. \tag{5}$$

Here m is the pollen mass in kg. Solving this differential equation analytically assuming spherical pollen grains with radius r (in m) yields

$$p_T(t_m) = p_a + \Delta\pi\left[1 - \exp\left(-\frac{3Ek}{r}\frac{\rho_w}{\rho_0}t_m\right)\right]. \tag{6}$$

Equation 6 calculates the turgor pressure that is reached after a given modeling time step t_m for each pollen grain in one gridbox, using the density of the pollen ρ_0 in $kg\ m^{-3}$. At the beginning of a time step, the turgor pressure

is assumed equal to the ambient atmospheric pressure ($p_T(0) = p_a$). Thus, the turgor pressure at the end of the timestep needs to translate to a burst fraction of the pollen grains (to be considered consumed for the next timestep). Zhou (2014) states that this requires a better understanding of the pollen wall strength. In the present study, we represent the pollen wall strength by a critical turgor pressure $p_{T,final}$ at which a single pollen grain bursts and which depends on the pollen type. The ratio between the actual turgor pressure increase to this critical turgor pressure increase $\left(\frac{p_T(t_m)-p_a}{p_{T,final}-p_a}\right)$ determines the burst fraction. We assume the total turgor pressure increase to distribute randomly amongst the pollen within an air volume. To simulate this, we apply an error function with an underlying Gaussian function which are chosen to ensure that $\mu \pm 3\sigma$ covers the total range of relevant turgor pressure values from $p_{T,min}$ where the pollen grain reaches its maximum volume, to $p_{T,final}$ where a single pollen grain is expected to burst. We interpret the results as the portion of pollen grains which burst into SPPs. Note, that in this study only birch pollen are considered to determine $p_{T,final}$. Birch pollen are found to release their SPPs through abortive germination (Grote et al., 2003) or a bursting of the pollen wall without prior germination (Suphioglu et al., 1992). Since germination generally involves a more time-consuming development of a pollen tube prior to release of SPPs (up to hours) we assume here the process of SPP release to occur by pollen bursting only. However, only birch pollen germination is previously documented with a RH of $RH_g = 96\%$ where germination occurs (Taylor et al., 2004). Since this RH value is linked to the release of the pollen's inner material, it is used as a first approach for determining $p_{T,final}$. As described above the water flux into the pollen grain stops when water potential inside and outside the pollen grain are equal. According to Equation 1 this occurs when

$$p_T = \Delta\pi + p_a. \tag{7}$$

To calculate the critical turgor pressure the equation is applied to a RH_g-environment. With the RH given, the water potential of the ambient air can be calculated using the universal gas constant $R = 8.314\ \mathrm{J\ mol^{-1}\ K^{-1}}$, ambient air temperature T in K and the molar volume of liquid water $M_W = 1.807 \cdot 10^{-5}\ \mathrm{m^3\ mol^{-1}}$ via

$$\pi_{out} = RT\frac{\ln \mathrm{RH}}{M_W}. \tag{8}$$

This equation is further used to determine the osmotic potential (π_{in}), where the water activity (a_w) of the swollen pollen grain replaces RH. Assuming $\Delta r_{max} = 1\ \mu\mathrm{m}$ as the maximum change in radius of the swelling birch pollen grain, the initial water activity ($a_{w,init} = 80\%$ (Zhou, 2014)) increases due to the water influx and according to the conservation of the amount of SPPs inside the pollen grain (Zhou, 2014)

$$C_0V_0 = C_1V_1 \quad \text{with} \quad C = -\frac{\pi}{RT}, \tag{9}$$

with the concentration of dissolved material C in $\mathrm{mol\ m^{-3}}$, the pollen grain volume V in $\mathrm{m^3}$, and the indices 0 and 1 referencing two points in time, to a value of $a_{w,final} = 84.5\%$. This implies the RH of the ambient air to exceed $RH_{min} = 84.5\%$ in order for the turgor pressure to increase. These two extreme values for the RH (RH_g and RH_{min}) are used to calculate the maximum ($p_{T,final}$) and minimum turgor pressure ($p_{T,min}$), respectively by applying Equation 7. We note that, assuming only pollen bursting, neglecting the more time-consuming abortive germination process, and translating an increasing turgor pressure into a pollen burst fraction is only a first approximation of the more complex underlying processes of pollen bursting. Table 1 lists all relevant parameters with their chosen values for the parameterization in this study, which is visualized in Figure 1. Figure 1 shows the temporal development of the turgor pressure (black) and the resulting fraction of bursted pollen (green) exemplary for three environments differing in ambient RH: 94% (solid), 96% (dotted), and 98% (dashed).

The number of SPPs released per bursted pollen grain is determined by their size. The generated SPPs are log-normally distributed, with the initial median diameter for the number concentration and mass concentration being 0.844 and 1.16 µm, respectively. The standard deviation for the size distribution is assumed to be 1.385. These values are based upon the findings of Sénéchal et al. (2015). The contribution of differing densities between pollen and SPP is expected to be negligible compared to their size differences, as these are both greater and used in the third power. Hence equal density for pollen and SPP is assumed. Further assuming no mass of material lost in the bursting process, applying the number distribution yields

$$\frac{N_{spp}}{N_{poll}} = \frac{\rho_{poll}}{\rho_{spp}}\left(\frac{d_{poll}}{d_{spp,N}}\right)^3 \exp\left[-4.5(\ln\sigma)^2\right] \approx 8260. \tag{10}$$

Table 1
Overview of Parameter Values for the Pollen Bursting Parameterization

Parameter	Value	Unit	Description
r_{poll}	$10.0 \cdot 10^{-6}$	m	Radius of birch pollen
Δr_{max}	$1.0 \cdot 10^{-6}$	m	Maximum swelling of pollen
$r_{spp,0}$	$0.422 \cdot 10^{-6}$	m	Median radius for SPP number concentration
$r_{spp,3}$	$0.58 \cdot 10^{-6}$	m	Median radius for SPP mass concentration
k	$5.0 \cdot 10^{-17}$	m s^{-1} Pa^{-1}	Water permeability of pollen Zhou (2014)
E	$2.15 \cdot 10^{9}$	N m^{-2}	Compression module of water
ρ_w	997	kg m^{-3}	Density of water
ρ_0, ρ_{poll}, ρ_{spp}	810	kg m^{-3}	Density of birch pollen (and SPP)
RH_{min}	84.5	%	Minimum relative humidity for p_T increase
RH_g	96	%	Maximum relative humidity for pollen burst
μ	0.5		Expectation of Gaussian distribution
σ	0.182		Standard deviation of Gaussian distribution

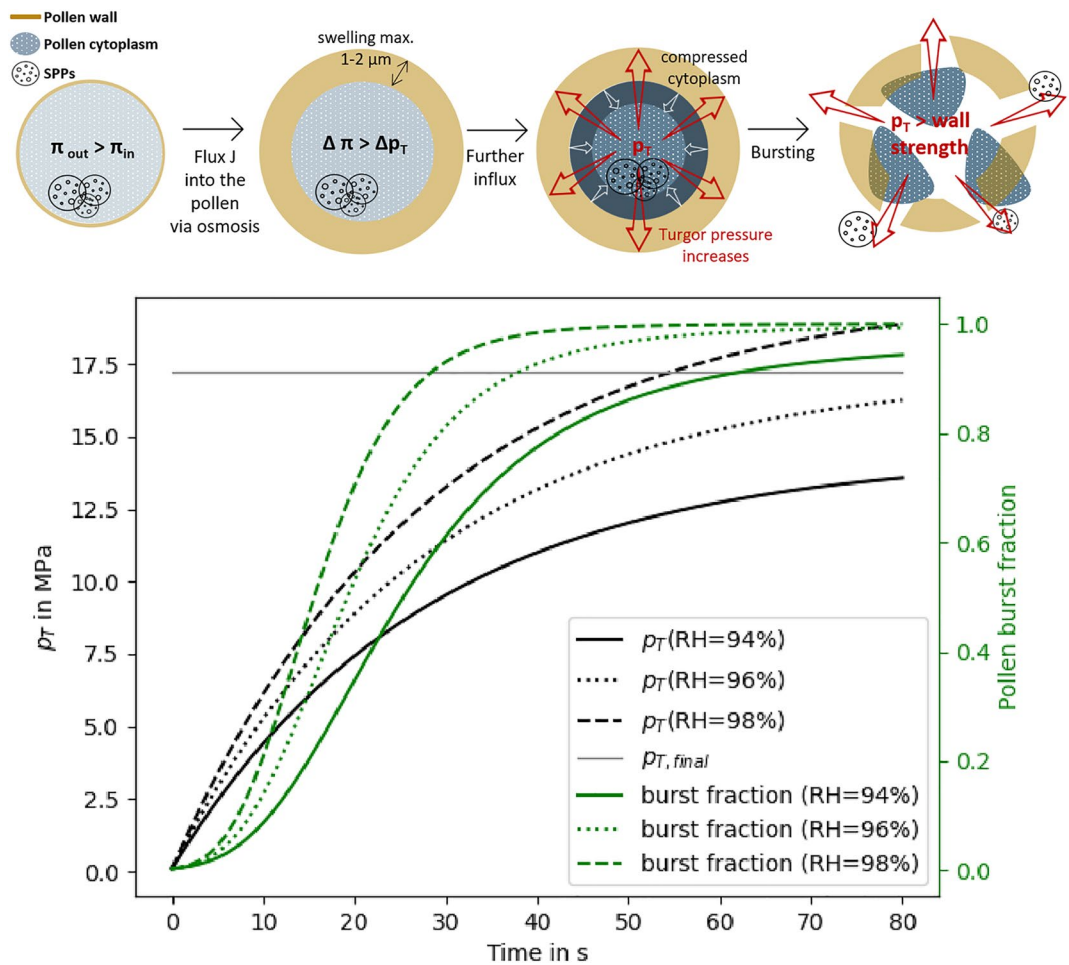

Figure 1. Schematic and temporal development of turgor pressure (black) and the fraction of bursted pollen (green) for the developed parametrization with p_a = 1,000 hPa, T = 293 K and (solid) RH = 94%, (dotted) RH = 96%, and (dashed) RH = 98%. The gray line indicates $p_{T,final}$.

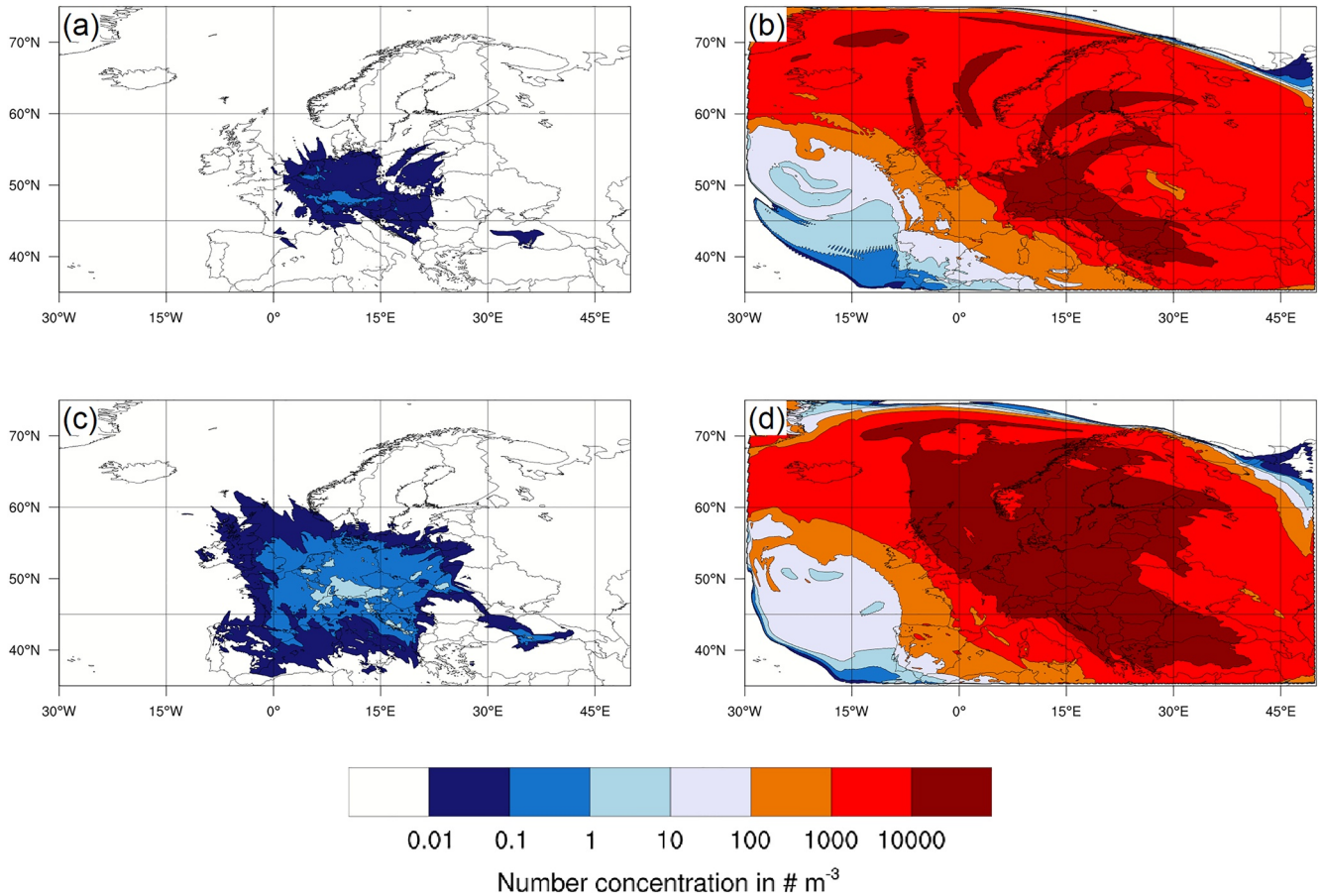

Figure 2. Horizontal distribution of pollen (left) and subpollen particle (right) averaged over the entire simulation period at 2,000 m (bottom) and 4,000 m (top) above ground.

This value probably overestimates the actual number of SPPs released per pollen grain in reality, since the grain's outer wall (the exine) does likely not contribute to SPP numbers generated during the bursting process.

2.2. Parameterization of Biological Ice Nucleation

The parameterization for biological ice nucleation (Phillips et al., 2013) which is implemented in ICON-ART (Rieger et al., 2017) and used in this study includes and considers primary biological aerosol particles as a separate group of INPs which is a development from previous parameterizations, that is, Phillips et al. (2008) where biological INPs were bulked together with all insoluble organics. Biological ice nucleation is assumed to contribute 3% toward a reference spectrum of the total INP concentration and occurs at high sub-zero temperatures below −2°C, while full nucleation efficiency of biological ice nuclei is reached at temperatures below −5°C. Ice nucleation efficiency is interpolated for the temperature range of $-5°C < T < -2°C$. Derived from observations, a proportionality is assumed between the concentrations of active INPs and aerosol total surface area (Phillips et al., 2013). In the context of this study, the biological particles acting as INPs are SPPs carrying ice nucleating macromolecules released from pollen grains through bursting as described above. Due to their low relevance for ice nucleation processes, pollen grains are not considered as INPs.

2.3. Model Configuration

In this study, the ICON-ART model is used in "Limited Area Mode" (LAM) with the area on which it operates covering large parts of Europe (see Figure 2), up to an altitude of 75,000 m. Two model simulations are performed: (a) a control simulation (referred to as simulation CTRL), where biological ice nucleation is disabled

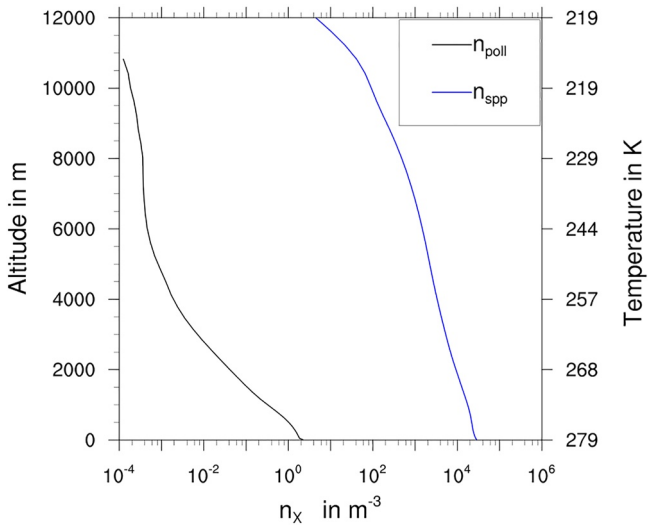

Figure 3. Mean vertical profiles of pollen (black) and subpollen particle (blue) number density. The ordinates show the altitude on the left and indicates the mean temperature at those altitudes on the right side.

and (b) a simulation with enabled biological ice nucleation and SPPs acting as INPs (referred to as simulation SPP). It is noted that in the CTRL simulation, ice formation is caused by homogeneous freezing and heterogeneous ice nucleation by a constant mineral dust background of $3 \cdot 10^6$ m^{-3}. Both simulations are performed on a grid with an equivalent grid size of 5 km and a time step of $\Delta t = 10$ s for 10 days starting on 29 March 2014 with no prior spin-up phase. The start date of the simulation corresponds to the onset of peak birch pollen emission season. The 2014 pollen season in the studied region is considered a so-called mast year for birch, that is, with high atmospheric birch pollen concentrations. The time period (dates and length) in combination with a large operating area was chosen for its variable synoptic situation. Multiple cyclones pass through the operating area during the time period advecting new air masses. While the first days show a small blocking situation in the central part of the domain, the blocking dissolves quickly for the rest of the time period. Precipitation events occur throughout the domain differing in duration and amount and temperature values show great spatial and temporal variation.

The boundary data for the LAM simulations were generated by a preceding global ICON-ART simulation and are read in once a day at 00:00 UTC. These model simulations include information on meteorological variables while pollen grain concentrations are unavailable for boundary data. The SPPs generated through pollen bursting using the parametrization described in the previous paragraphs act exclusively as INPs while CCN are prescribed with a constant background concentration of $2 \cdot 10^8$ m^{-3}. Birch pollen are the only pollen grain type emitted in this study and thus the only interactive aerosol and source of SPPs in the simulations presented here. The pollen grains have a diameter of 20 µm.

For further assessment of the SPPs' potential on ice nucleation, impact sensitivity tests were performed. Artificial factors are applied to the result of the ice nucleation parameterization, namely the amount of new ice particles formed by the SPPs, equating in an increase in the SPP's ice nucleation efficiency. These factors are 10^1, 10^2, 10^3, 10^4, and 10^5, while not exceeding the maximum number of SPPs available as INPs. The corresponding model simulations are in the following referenced as SPP_x10, SPP_x100, SPP_x1000, SPP_x10000, and SPP_x100000, respectively.

3. Results

3.1. Spatial Distribution of Pollen and SPPs

For SPP concentration and distribution we generally find that SPP number concentrations exceed those of pollen grains by orders of magnitude at different altitude levels as shown in Figures 2a and 2b for 4,000 m and Figures 2c and 2d for 2,000 m above ground, respectively. Further, SPPs extend over a significant larger area than pollen grains, as evident from the horizontal distribution of pollen and SPP number concentrations averaged over the simulation period (Figure 2). Pollen concentrations over Scandinavia and Eastern Europe are negligible due to the respective pollen seasons not having started yet. Vertical profiles of pollen and SPP density (Figure 3) show that high SPP concentrations prevail at higher altitudes while pollen grain concentration decreases rapidly with increasing altitude. At 4,000 m, an altitude where the temperature is typically below 268 K, thus in a range where biological ice nucleation occurs, vertical profiles further highlight the abundance of SPPs with $\overline{n_{spp}} \approx 4 \cdot 10^3$ m^{-3} and the scarcity of pollen grains with $\overline{n_{poll}} \approx 3.4 \cdot 10^{-3}$ m^{-3}. Both findings, horizontal and vertical extent of SPP and pollen, are governed by sedimentation, where the settling velocity of SPPs is much smaller than that of pollen grains with a subsequently higher atmospheric lifetime of SPPs compared to pollen grains.

3.2. Impact of SPPs on Ice Particle and Cloud Droplet Number Concentration

To assess the impact of SPPs on ice particle number concentrations, we use joint histograms of the absolute occurrence of SPP concentration n_{spp} and ice particle number density n_i for the CTRL simulation in Figure 4a and the SPP simulation in Figure 4b. The histograms consider model results at each grid point and the entire simulation

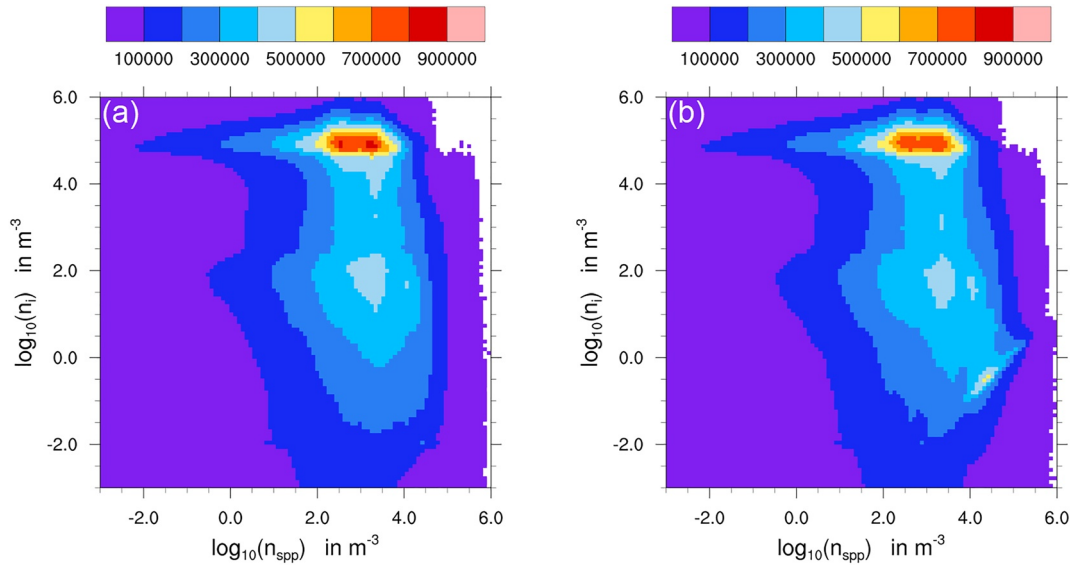

Figure 4. Joint histograms of n_i and n_{spp} for the simulations (a) CTRL and (b) subpollen particle (SPP) for all grid points and the complete simulation period. The absolute occurrence of ice particle number density n_i and SPP concentration n_{spp} is color coded.

period. A temperature filter is applied, such that only data occurring below $T = 274$ K are considered. The histogram of the CTRL simulation (Figure 4a) shows a strong mode in the ice particle number concentration of around 10^5 m^{-3} which can be attributed to homogeneous freezing and ice formation initiated by a constant background of mineral dust INPs. The temperature at the contributing grid points is predominantly below 243 K, in most cases even below 233 K (not shown here) where homogeneous ice nucleation is the dominant freezing mechanism. Interestingly, the high ice particle number concentrations concur with high SPP number concentrations.

When biological ice nucleation is enabled (simulation SPP shown in Figure 4b), an additional mode at lower values of ice particle number concentration of around 10^{-2}–10^{1} m^{-3} appears. This mode shows a correlation, indicating that an increase in SPP concentration is linked to an increase in ice particle number density. As biological ice nucleation is effective at higher temperatures than other types of ice nucleation, it is reasonable to propose that this biological mode affects low-level clouds at generally higher temperatures.

For further investigation, we take a closer look at the spatially and temporally averaged vertical profiles of ice particle number density n_i shown in Figure 5a for simulations CTRL (dashed curve) and SPP (solid curve) and the relative deviation between the two profiles shown in Figure 5b. Overall, the profiles of simulations CTRL and

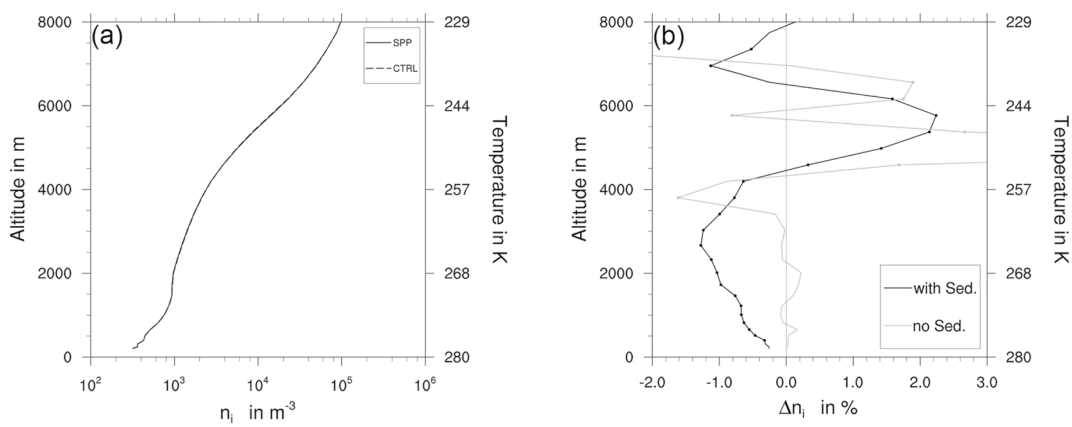

Figure 5. Mean profiles of (a) ice particle number density of and (b) relative difference between the simulations subpollen particle (SPP) and CTRL.

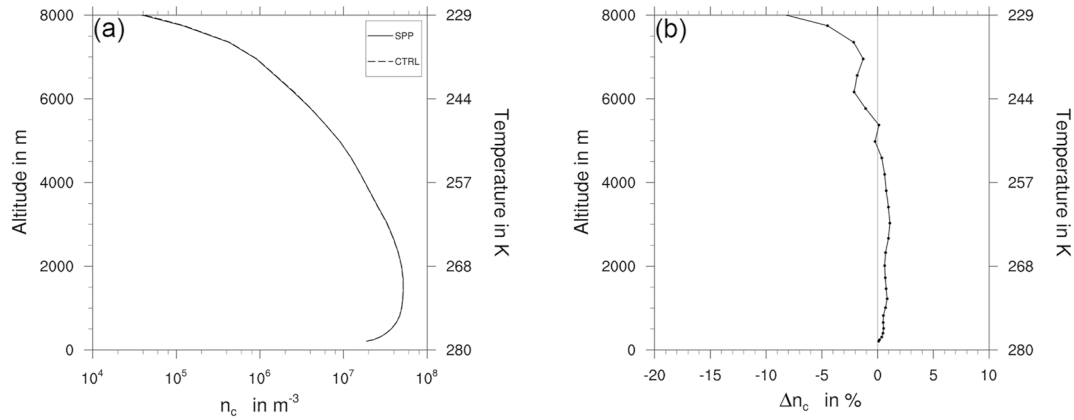

Figure 6. Mean profiles of (a) cloud droplet particle number density of and (b) relative difference between the simulations subpollen particle and CTRL.

SPP differ only slightly where statistically significant segments in the profile of relative difference between the two simulations (marked with a dot following a Student's-T-test) cover the entire profile. What is interesting is that the ice particle number density in the lower altitude levels is smaller in simulation SPP compared to CTRL. In fact, one would expect the contrary, higher ice particle number density in lower altitudes, as biological ice nucleation is already active at those lower altitude levels with generally higher temperatures compared to higher altitudes. We hypothesize that the reduction in ice particle number density is caused by changes in ice particle sedimentation. To confirm this assumption, modified SPP- and CTRL-simulations, where hydrometeor sedimentation is suppressed, were performed, and show the above mentioned expected behavior of a slight increase in ice particle number density in the lower levels (up to about 0.2%, Figure 5b). Without this artificial suppression of sedimentation, ice particles generally form at higher altitudes and subsequently sediment. Now, SPP generation adds additional biological INPs leading to more but smaller ice particles. Small particles generally sediment slower than large particles and subsequently, at a given time step, less ice particles are provided to lower altitudes. In the setup of this study, the reduction of ice particles through sedimentation outweighs the increase in ice particles by biological ice nucleation from the added SPPs at lower altitudes. At higher altitudes around 6,000 m, the ice particle number density in the simulation SPP exceeds those of CTRL by a maximum value of around 2%. Although the biological INPs compete with non-biological INPs (i.e., mineral dust), in this altitude the added number of SPP INPs from pollen bursting and the slower settling of the resulting smaller ice particles result in an overall higher ice particle number density in the higher altitude.

Contrary to the ice particle number densities, cloud droplet number concentration n_c (Figure 6) show higher values in the lower altitude regions and a decrease of droplet concentration with increasing altitude (Figure 6b); while the mean profiles of the cloud droplet number concentration indicate negligible differences between the CTRL- and the SPP-simulations.

A maximum increase of cloud droplet number concentration is reached at about 3,000 m with a relative value of about 1%. The higher number density of cloud droplets in lower altitudes can be explained by indirect or secondary effects where the low ice particle number density weakens other microphysical processes, for example, riming, hence, lowering cloud droplet consumption. Conversely, at higher altitudes, where a small increase in ice particle number density is found, the cloud droplet number density is reduced.

3.3. Sensitivity to Ice Nucleation Efficiency

So far we saw that considering SPPs as biological INPs only leads to small changes in ice particle and cloud droplet numbers (Figures 5b and 6b). Yet, the changes in ice particle and cloud droplet numbers induced by SPPs are statistically significant. We conducted sensitivity tests, as described in Section 2, to further investigate SPP ice nucleation efficiencies and to identify potential thresholds where SPP become prominent INPs for the production of cloud ice and droplets.

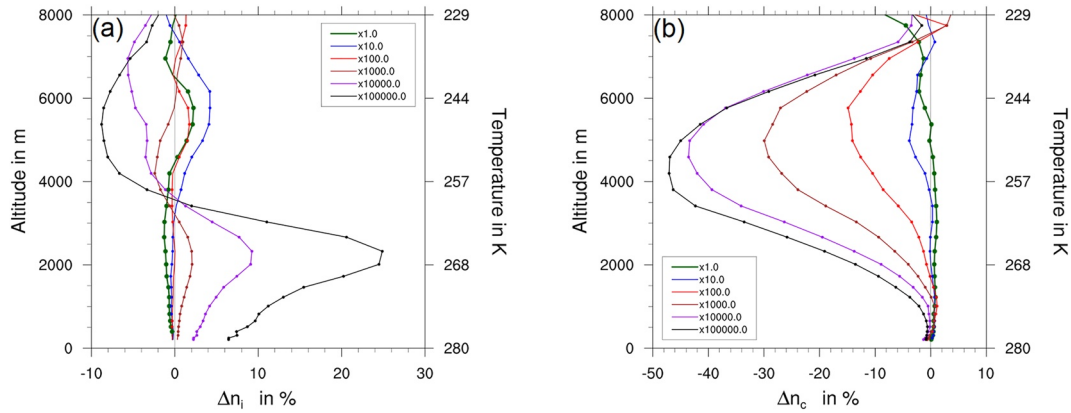

Figure 7. Profile of relative difference of (a) ice particle number density and (b) droplet number density between simulations subpollen particle and CTRL for various sensitivities.

The impact factor multiplication of ice particle numbers has on the ice particle and the cloud droplet number density is shown in Figure 7a and Figure 7b, respectively. Efficiency factors are color coded (see figure legend) in relation to the reference SPP-simulation (shown in green).

The previously described effect of slowed sedimentation to lower altitudes by additional ice particles from SPP ice nucleation remains relevant up to a multiplication factor of 100 (Figure 7a). At higher nucleation efficiencies, ice particle numbers significantly increase in the lower altitudes while decreasing in higher regions above 4,000 m. A clear maximum increase in ice particle numbers is reached just above 2,000 m. The profile of increased ice particle loads in low altitudes and reduced ice particle loads in higher regions can be explained by the humidity already being largely consumed at lower levels by the increased ice nucleation from SPPs combined with a suppression of nucleation processes in higher levels by hydrometeors already being present.

For droplet number densities, Figure 7b indicates that the transition from increase to reduction of droplet number density moves to lower altitudes with increasing biological ice nucleation efficiency. Additionally, the amplitude of the reduction increases and the highest reduction in droplet number density is found at around 5,000 m. The increased ice particle number density (Figure 7a) causes the reduction in droplet number density in the lower altitudes, as ice nucleation consumes humidity which is subsequently no longer available for droplet formation and further nucleation is suppressed by hydrometeors already being present. Additionally, the abundance of ice particles enhances microphysical processes like riming, that further consumes droplets. The aforementioned turning point of biological ice nucleation efficiency for the ice particle number density (SPP_x100) has no comparable role when regarding the cloud droplet number density. However, it shows a substantial reduction of more than 10%.

3.4. Impacts of SPP on Precipitation Rates

We further investigated the impact of SPPs on the water budget with results shown in Figure 8 where Figure 8a shows profiles of absolute differences in water vapor mass concentration between the simulations SPP and CTRL and Figure 8b shows the relative change in accumulated precipitation ($\Delta RR_{akk,rel}$) at the end of the simulation period for various sensitivity factors.

Comparable to the solid and liquid phases, the gaseous phase is only slightly impacted for sensitivity factors up to 100. Here the lower levels are drier when SPPs as biological INPs are considered. This humidity reduction diminishes with increasing altitude and for the SPP and the SPP_x10 simulations even shifts into a humidifying effect, peaking at around 2,500–3,000 m concurring with the decrease in ice particle number concentration. At higher sensitivity factors the described effects shift: The lower 1,200 m show a strong increase in water vapor, having the maximum increase at an altitude between 500 and 1,000 m. This is explained by the hydrometeors being smaller due to the increased particle number densities and therefore being more susceptible to evaporation and sublimation in these warmer parts of the atmosphere. Above 1,200 m the effect changes sign and the atmosphere is therefore drier in the SPP simulations compared to CTRL, peaking at around 3,000 m, due to higher

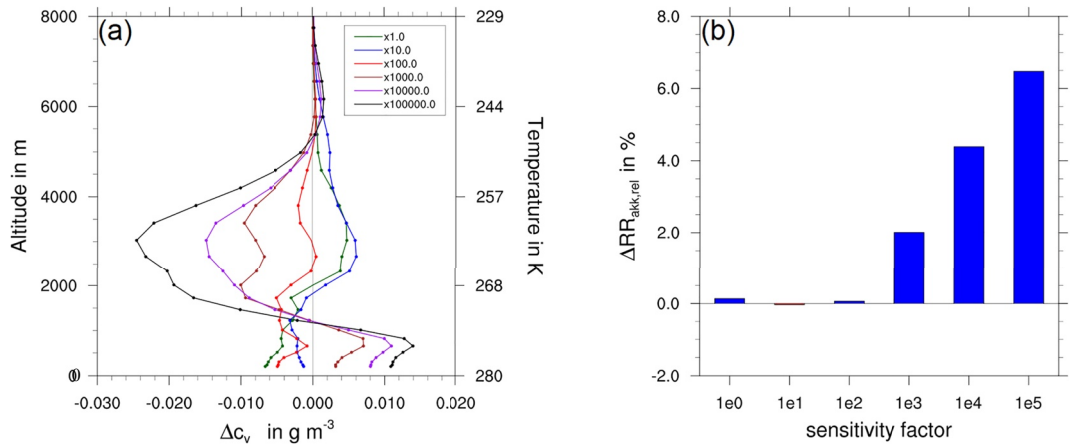

Figure 8. (a) Profiles of absolute difference in mass concentration for water vapor and (b) relative change in total precipitation for various nucleation efficiency sensitivities.

consumption of humidity by the additional nucleation processes and the growth of those increased hydrometeor number densities.

For higher sensitivity factors (above SPP_x100) the atmosphere becomes considerably drier overall. The lower sensitivity factors, however, don't seem to affect the overall atmospheric water budget considerably. Figure 8b confirms the previous findings, as it shows the relative difference of total accumulated precipitation at the end of the simulation period between the simulations SPP and CTRL for the different sensitivity factors. No notable change is found for SPP_x1, SPP_x10, and SPP_x100. However, SPP_x1000, SPP_x10000, and SPP_x100000 result in 2%, 4.5%, and 6.5% increased precipitation respectively, supporting the previously found loss in atmospheric water content.

It is noted, that although the sensitivities are applied to the ice nucleation efficiency, comparable effects can be seen by applying the sensitivities to the SPP number concentration directly and hereby influencing the effect of pollen bursting.

3.5. Comparison With Laboratory Results and Uncertainties

The previous parts showed that, although the reference SPP simulation has no substantial impact on atmospheric water, increasing ice nucleation efficiency is found to show relevant impacts on atmospheric water. Particularly ice nucleation efficiency factor 100 seems relevant as it marks a turning point. Factors beyond 100 lead to considerable changes in ice particle and cloud droplet number concentrations in relevant altitudes.

Generally, in simulations, the extent to which biogenic ice nucleation, for example, from SPPs, impacts ice particle and cloud droplet number concentrations strongly depends on the capability of the applied ice nucleation parameterization to represent different INP types and the subsequently achieved ice nucleation rates. To put the parameterization used in this study, which is not specific for SPP, to the test, we compare to experimental evidence. Using recent experimental data for silver birch SPPs acting as INPs we derive an upper limit for the number concentration of INPs for SPPs as $n_{INP} = 0.035\ m^{-3}$, for a SPP mass concentration of 1.2 µg kg^{-1}. This SPP mass concentration is the maximum value found in the modeled output of the SPP parameterization. Here, the INP value per milligram carbon at the median freezing temperature is used in conjunction with an assumed carbon to oxygen ratio of 1:1. This ratio is appropriate for polysaccharides, which the SPPs likely consist of (Dreischmeier et al., 2017). To our knowledge, this is the first data set available for pollen INPs where the INP concentration in air can be calculated from the reported number of INPs per mass organic carbon. The study used filtered pollen samples with sizes smaller than 0.45 µm. This direct comparison suggests, that even with non-factored nucleation efficiencies the simulated INP concentrations from birch SPPs may be overestimated by at least one order of magnitude when using the biological ice nucleation parameterization as described by Phillips et al. (2013).

Reflecting on uncertainties in the SPP simulation, the probably most prominent uncertainty stems from the fact that only one pollen type is considered, namely birch pollen and birch SPPs from pollen bursting. Thus, the simulation does not fully represent the entire pollen and subsequently SPP load. The size of the represented and especially unrepresented pollen and SPP is a further uncertainty. The smaller the SPPs are, the more are generated by the bursting process, and the easier they are transported. Although the consequently reduced SPP's surface influences its ice nucleation rate, the increased numbers outweigh that effect. Additionally, the unrepresented pollen may have a lower critical RH value for the bursting process or a lower minimum RH value for turgor pressure to build up. The critical RH itself likely adds to the overall uncertainty in simulating SPPs, as it is used to estimate the pollen wall strength in the bursting process. Potentially weakening influences on the pollen wall strength (e.g., wind stress, chemical processes) are also neglected in the conducted simulation. The minimum RH is solely derived from the maximal swelling of the pollen and does not take into account other potential conditions for water intake. Furthermore, real pollen would not be totally converted into spherical SPPs as the parameterization suggests, since at least parts of the pollen wall would remain intact and the SPPs released are more irregularly shaped. As for the INP parameterization used in this study, the same issue of only considering one pollen type (when comparing to experimental results) poses potential for large uncertainties, suggesting the parameterization being dominated by more IN active biological material than SPPs, that is, bacteria.

Thus, while direct comparison with experimental results for birch SPP INPs suggests that the simulation overestimates INPs from birch SPP, its uncertainties justify the introduction and consideration of the sensitivity factors.

4. Summary and Discussion

Biological ice nucleation is amongst the most efficient forms of ice formation. However, due to the inability of the corresponding INPs (e.g., pollen) to reach relevant altitudes due to their large size and mass, the process is assumed to be mostly insignificant in most atmospheric regions. For the first time, this study investigated the effects of subpollen particles on the overall ice nucleation, as SPPs with their smaller size compared to intact pollen grains can reach ice nucleation relevant altitudes. These SPPs form as the result of pollen bursting, which occurs when the pollen grains enter environments of high humidity. In this study, we used the ICON-ART model and present a newly developed pollen burst parameterization to calculate the emission and dispersion of (birch) SPPs and to simulate their effects on ice nucleation, cloud droplets, and precipitation over Europe over the course of 10 days. Thus, this study extends our understanding of SPP contributions to cloud processes as previous studies thus far only focused on SPPs as CCN.

In the following, we summarize our findings along the three research questions we stated in the introduction: First, answering the question of *How high are SPP concentrations throughout the troposphere*?, we generally found that SPP concentrations exceed those of pollen grains by several orders of magnitude at different altitude levels. Near ground level, this has implications on the atmospheric load of allergen material where the smaller SPPs ($\overline{n}_{\mathrm{spp,ground}} \approx 3 \cdot 10^4\ \mathrm{m}^{-3}$) might lead to more adverse health effects as they can more easily penetrate the human respiratory system, for example, the previously mentioned Thunderstorm Asthma. On the effects of pollen and SPPs on cloud processes, we found high SPP number concentrations in altitudes with temperatures just below freezing, where SPP concentrations are multiple orders of magnitude higher than the number concentration of pollen (around $4 \cdot 10^3\ \mathrm{m}^{-3}$ at 4,000 m compared to $3 \cdot 10^{-3}\ \mathrm{m}^{-3}$ for pollen). This deviation between pollen and SPP concentration as well as the amount of SPP generated per pollen grain agree well with the SPP_LIT/SPP_LOW experiment in the study by Wozniak et al. (2018). However, we note that SPP concentrations in our study are several orders of magnitude lower than values reported by the previous study (Wozniak et al., 2018). We attribute the lower SPP concentrations to a reduced value of pollen concentration, as the SPPs generated per pollen grain are comparable.

Second, on the question *Do SPPs have a significant impact on the amount of ice formed in mixed-phase clouds*?, we find the formation of a new ice particle mode at higher temperatures indicating its biological nature when considering SPPs as potential INPs. The effect on the mean profile of ice particle number density, however, is small (ranging from -1.2% to 2.2%) and qualitatively unexpected, as it is reduced at higher temperatures and increased in lower temperatures. This is due to the change in sedimentation behavior of the ice particles, which counteracts the direct effect on ice nucleation in those altitudes.

Lastly, answering the question on *How does this* (*the impact of SPPs on ice formation in mixed-phase clouds*) *affect precipitation*? and thus the question of the paper title when SPPs become relevant for ice nucleation processes in clouds, we find that the effect on cloud droplet number density is similarly small and due to the indirect effect on sedimentation positive. However, the effects are statistically significant. A sensitivity investigation yields, that at an increased ice nucleation efficiency of about 100 the sedimentation effects are mostly compensated. Higher ice nucleation efficiencies further lead the biological mode to manifest at lower altitudes (2,000–4,000 m) with increases in ice particle number density of up to 25% and a reduction above 4,000 m of up to 8%. The cloud droplet density, contrarily, experiences a reduction throughout the analyzed lowest 8,000 m of altitude (peaking at around 4,000 m for −46%). This can be explained by a reduced cloud droplet nucleation due to consumption of humidity for ice nucleation and enhanced microphysical effects like riming or the Wegener-Bergeron-Findeisen-process. This reduction, caused by the increased ice nucleation rates, dominates the change in atmospheric water, which leads to an increase in overall precipitation of up to 6.2%.

This is the first study to present a physically based pollen bursting parameterization for application in an operational weather forecast model—here ICON-ART—and in combination with an INP parameterization for the resulting SPPs. While values calculated from the simulation and experimental data show some deviation they demonstrate a promising start and highlight the importance to better understand different biological INPs and their emission processes into the atmosphere.

Conflict of Interest

The authors declare no conflicts of interest relevant to this study.

Data Availability Statement

The output data from the ICON-ART simulations performed for identifying the role of SPPs in the study are available at RADAR4KIT via https://doi.org/10.35097/830 licensed with, "CC BY-NC-ND 4.0" (Werchner, 2021). The used ICON-ART code is license protected and can be accessed by request to the corresponding author.

Acknowledgments
This work was performed on the computational resource ForHLR II funded by the Ministry of Science, Research and the Arts Baden-Württemberg and Deutsche Forschungsgemeinschaft (DFG). Furthermore resources of the Deutsches Klimarechenzentrum (DKRZ) granted by its Scientific Steering Committee (WLA) under Project ID bb1070 have been used. EG received funding from the University of Toronto Scarborough Department of Physical and Environmental Sciences Travel Award. CH has received funding from the European Research Council (ERC) under the European Union's Horizon 2020 research and innovation programme under Grant 714062 (ERC Starting Grant "C2Phase") and 821205 ("FORCeS"). Open Access funding enabled and organized by Projekt DEAL.

References

Bacsi, A., Choudhury, B. K., Dharajiya, N., Sur, S., & Boldogh, I. (2006). Subpollen particles: Carriers of allergenic proteins and oxidases. *The Journal of Allergy and Clinical Immunology*, *118*(4), 844–850. https://doi.org/10.1016/j.jaci.2006.07.006

Baklanov, A., Smith Korsholm, U., Nuterman, R., Mahura, A., Nielsen, K. P., Sass, B. H., et al. (2017). Enviro-HIRLAM online integrated meteorology–chemistry modelling system: Strategy, methodology, developments and applications (v7.2). *Geoscientific Model Development*, *10*(8), 2971–2999. https://doi.org/10.5194/gmd-10-2971-2017

Burkart, J., Gratzl, J., Seifried, T. M., Bieber, P., & Grothe, H. (2021). Isolation of subpollen particles (SPPs) of birch: SPPs are potential carriers of ice nucleating macromolecules. *Biogeosciences*, *18*(20), 5751–5765. https://doi.org/10.5194/bg-18-5751-2021

Després, V. R., Huffman, J. A., Burrows, S. M., Hoose, C., Safatov, A., Buryak, G., et al. (2012). Primary biological aerosol particles in the atmosphere: A review. *Tellus B: Chemical and Physical Meteorology*, *64*(1), 15598. https://doi.org/10.3402/tellusb.v64i0.15598

Dreischmeier, K., Budke, C., Wiehemeier, L., Kottke, T., & Koop, T. (2017). Boreal pollen contain ice-nucleating as well as ice-binding 'antifreeze' polysaccharides. *Scientific Reports*, *7*(1), 41890. https://doi.org/10.1038/srep41890

Fröhlich-Nowoisky, J., Kampf, C. J., Weber, B., Huffman, J. A., Pöhlker, C., Andreae, M. O., et al. (2016). Primary biological aerosol particles in the atmosphere: A review. *Atmospheric Research*, *182*(1), 346–376. https://doi.org/10.3402/tellusb.v64i0.15598

Gasch, P., Rieger, D., Walter, C., Khain, P., Levi, Y., Knippertz, P., & Vogel, B. (2017). Revealing the meteorological drivers of the September 2015 severe dust event in the Eastern Mediterranean. *Atmospheric Chemistry and Physics*, *17*(22), 13573–13604. https://doi.org/10.5194/acp-17-13573-2017

Giorgetta, M. A., Brokopf, R., Crueger, T., Esch, M., Fiedler, S., Helmert, J., et al. (2018). ICON-A, the atmosphere component of the ICON Earth system model: I. Model description. *Journal of Advances in Modeling Earth Systems*, *10*(7), 1613–1637. https://doi.org/10.1029/2017MS001242

Grote, M., Valenta, R., & Reichelt, R. (2003). Abortive pollen germination: A mechanism of allergen release in birch, alder, and hazel revealed by immunogold electron microscopy. *The Journal of Allergy and Clinical Immunology*, *111*(5), 1017–1023. https://doi.org/10.1067/mai.2003.1452

Gute, E., & Abbatt, J. (2020). Ice nucleating behavior of different tree pollen in the immersion mode. *Atmospheric Environment*, *231*, 117488. https://doi.org/10.1016/j.atmosenv.2020.117488

Hader, J. D., Wright, T. P., & Petters, M. D. (2014). Contribution of pollen to atmospheric ice nuclei concentrations. *Atmospheric Chemistry and Physics*, *14*(11), 5433–5449. https://doi.org/10.5194/acp-14-5433-2014

Hoose, C., Kristjánsson, J., & Burrows, S. (2010). How important is biological ice nucleation in clouds on a global scale? *Environmental Research Letters*, *5*(2), 024009. https://doi.org/10.1088/1748-9326/5/2/024009

Hoose, C., & Möhler, O. (2012). Heterogeneous ice nucleation on atmospheric aerosols: A review of results from laboratory experiments. *Atmospheric Chemistry and Physics*, *12*(20), 9817–9854. https://doi.org/10.5194/acp-12-9817-2012

Hoshyaripour, G. A., Bachmann, V., Förstner, J., Steiner, A., Vogel, H., Wagner, F., et al. (2019). Effects of particle nonsphericity on dust optical properties in a forecast system: Implications for model-observation comparison. *Journal of Geophysical Research: Atmosphere*, *124*(13), 7164–7178. https://doi.org/10.1029/2018JD030228

Huang, S., Hu, W., Chen, J., Wu, Z., Zhang, D., & Fu, P. (2021). Overview of biological ice nucleating particles in the atmosphere. *Environment International*, *146*, 106197. https://doi.org/10.1016/j.envint.2020.106197

Jacobson, M. Z., & Streets, D. G. (2009). Influence of future anthropogenic emissions on climate, natural emissions, and air quality. *Journal of Geophysical Research*, *114*(D8), D08118. https://doi.org/10.1029/2008JD011476

Lüttge, U., & Kluge, M. (2012). *Botanik - Die einführende biologie der Pflanzen* (6 aktualisierte ed.). Wiley VCH.

O'Sullivan, D., Murray, B. J., Ross, J. F., Whale, T. F., Price, H. C., Atkinson, J. D., et al. (2015). The relevance of nanoscale biological fragments for ice nucleation in clouds. *Scientific Reports*, *5*(1), 8082. https://doi.org/10.1038/srep08082

Pauling, A., Clot, B., Menzel, A., & Pratt, J. S. (2020). Pollen forecasts in complex topography: Two case studies from the Alps using the numerical pollen forecast model COSMO-ART. *Aerobiologia*, *36*(1), 25–30. https://doi.org/10.1007/s10453-019-09590-2

Phillips, V. T., DeMott, P. J., & Andronache, C. (2008). An empirical parameterization of heterogeneous ice nucleation for multiple chemical species of aerosol. *Journal of the Atmospheric Sciences*, *65*(9), 2757–2783. https://doi.org/10.1175/2007JAS2546.1

Phillips, V. T., Demott, P. J., Andronache, C., Pratt, K. A., Prather, K. A., Subramanian, R., & Twohy, C. (2013). Improvements to an empirical parameterization of heterogeneous ice nucleation and its comparison with observations. *Journal of the Atmospheric Sciences*, *70*(2), 378–409. https://doi.org/10.1175/JAS-D-12-080.1

Pummer, B., Bauer, H., Bernardi, J., Bleicher, S., & Grothe, H. (2012). Suspendable macromolecules are responsible for ice nucleation activity of birch and conifer pollen. *Atmospheric Chemistry and Physics*, *12*(5), 2541–2550. https://doi.org/10.5194/acp-12-2541-2012

Rieger, D., Bangert, M., Bischoff-Gauss, I., Förstner, J., Lundgren, K., Reinert, D., et al. (2015). ICON–ART 1.0–a new online-coupled model system from the global to regional scale. *Geoscientific Model Development*, *8*(6), 1659–1676. https://doi.org/10.5194/gmd-8-1659-2015

Rieger, D., Steiner, A., Bachmann, V., Gasch, P., Förstner, J., Deetz, K., et al. (2017). Impact of the 4 April 2014 Saharan dust outbreak on the photovoltaic power generation in Germany. *Atmospheric Chemistry and Physics*, *17*(21), 13391–13415. https://doi.org/10.5194/acp-17-13391-2017

Schäppi, G. F., Suphioglu, C., Taylor, P. E., & Knox, R. B. (1997). Concentrations of the major birch tree allergen Bet v 1 in pollen and respirable fine particles in the atmosphere. *The Journal of Allergy and Clinical Immunology*, *100*(5), 656–661. https://doi.org/10.1016/S0091-6749(97)70170-2

Schröter, J., Rieger, D., Stassen, C., Vogel, H., Weimer, M., Werchner, S., et al. (2018). ICON-ART 2.1: A flexible tracer framework and its application for composition studies in numerical weather forecasting and climate simulations. *Geoscientific Model Development*, *11*(10), 4043–4068. https://doi.org/10.5194/gmd-11-4043-2018

Sénéchal, H., Visez, N., Charpin, D., Shahali, Y., Peltre, G., Biolley, J.-P., et al. (2015). A review of the effects of major atmospheric pollutants on pollen grains, pollen content, and allergenicity. *The Scientific World Journal*, *2015*, 1–29. https://doi.org/10.1155/2015/940243

Sofiev, M., Berger, U., Prank, M., Vira, J., Arteta, J., Belmonte, J., et al. (2015). MACC regional multi-model ensemble simulations of birch pollen dispersion in Europe. *Atmospheric Chemistry and Physics*, *15*(14), 8115–8130. https://doi.org/10.5194/acp-15-8115-2015

Steiner, A. L., Brooks, S. D., Deng, C., Thornton, D. C., Pendleton, M. W., & Bryant, V. (2015). Pollen as atmospheric cloud condensation nuclei. *Geophysical Research Letters*, *42*(9), 3596–3602. https://doi.org/10.1002/2015GL064060

Suphioglu, C. (1998). Thunderstorm asthma due to grass pollen. *International Archives of Allergy and Immunology*, *116*(4), 253–260. https://doi.org/10.1159/000023953

Suphioglu, C., Singh, M. B., Taylor, P., Knox, R., Bellomo, R., Holmes, P., & Puy, R. (1992). Mechanism of grass-pollen-induced asthma. *The Lancet*, *339*(8793), 569–572. https://doi.org/10.1016/0140-6736(92)90864-Y

Taylor, P., Flagan, R., Miguel, A., Valenta, R., & Glovsky, M. (2004). Birch pollen rupture and the release of aerosols of respirable allergens. *Clinical and Experimental Allergy*, *34*(10), 1591–1596. https://doi.org/10.1111/j.1365-2222.2004.02078.x

Vogel, H., Pauling, A., & Vogel, B. (2008). Numerical simulation of birch pollen dispersion with an operational weather forecast system. *International Journal of Biometeorology*, *52*(8), 805–814. https://doi.org/10.1007/s00484-008-0174-3

Wang, J., Qi, M., Huang, H., Ye, R., Li, X., & Stewart, C. N. (2017). Atmospheric pollen dispersion from herbicide-resistant horseweed (Conyza canadensis L.). *Aerobiologia*, *33*(3), 393–406. https://doi.org/10.1007/s10453-017-9477-3

Werchner, S. (2021). Simulated concentration data for birch pollen, birch SPP, hydrometeors, and atmospheric variables [Dataset]. Karlsruhe Institute of Technology. https://doi.org/10.35097/830

Wozniak, M., Solmon, F., & Steiner, A. (2018). Pollen rupture and its impact on precipitation in clean continental conditions. *Geophysical Research Letters*, *45*(14), 7156–7164. https://doi.org/10.1029/2018GL077692

Zängl, G., Reinert, D., Rípodas, P., & Baldauf, M. (2015). The ICON (ICOsahedral Non-hydrostatic) modelling framework of DWD and MPI-M: Description of the non-hydrostatic dynamical core. *Quarterly Journal of the Royal Meteorological Society*, *141*(687), 563–579. https://doi.org/10.1002/qj.2378

Zhang, R., Duhl, T., Salam, J. M., House, M. T., Flagan, R. C., Avol, E. L., et al. (2013). Development of a regional-scale pollen emission and transport modeling framework for investigating the impact of climate change on allergic airway disease. *Biogeosciences*, *10*(3), 3977–4023. https://doi.org/10.5194/bg-11-1461-2014

Zhou, Q. (2014). Relative humidity induced plant pollen grain rupture and conceptual model development (Master's Thesis - Washington State University - May 2014).

Zink, K., Pauling, A., Rotach, M., Vogel, H., Kaufmann, P., & Clot, B. (2013). EMPOL 1.0: A new parameterization of pollen emission in numerical weather prediction models. *Geoscientific Model Development*, *6*(6), 1961–1975. https://doi.org/10.5194/gmd-6-1961-2013